Published in final edited form as:
J Neuroimaging. 2012 April ; 22(2): 184–190. doi:10.1111/j.1552-6569.2010.00561.x.

Comparison of proton magnetic resonance spectroscopy with fluorine-18 2-fluoro-deoxyglucose positron emission tomography for assessment of brain tumor progression

Farzin Imani, MD, PhD[1], **Fernando E. Boada, PhD**[1], **Frank S. Lieberman, MD**[2], **Denise K. Davis, BS**[1], **Erin L. Deeb, BS**[1], and **James M. Mountz, MD, PhD**[1]

[1]Department of Radiology, University of Pittsburgh Medical Center, Pennsylvania

[2]Department of Neurology, University of Pittsburgh Medical Center, Pennsylvania

Abstract

Objectives—We investigated the accuracy of high-field proton magnetic resonance spectroscopy (^{1}H-MRS) and fluorine-18 2-fluoro-deoxyglucose positron emission tomography (^{18}F-FDG-PET) for diagnosis of glioma progression following tumor resection, stereotactic radiation and chemotherapy.

Methods—Twelve post-therapy patients with histology proven gliomas (6 grade II and 6 grade III) presented with Magnetic Resonance Imaging (MRI) and clinical symptoms suggestive but not conclusive of progression were entered into the study. ^{1}H-MRS data were acquired and 3D volumetric maps of choline (Cho) over creatine (Cr) were generated. Intensity of ^{18}F-FDG uptake was evaluated on a semiquantitative scale.

Results—The accuracy of ^{1}H-MRS and ^{18}F-FDG-PET imaging for diagnosis of glioma progression was 75% and 83% respectively. Classifying the tumors by grade improved accuracy of ^{18}F-FDG-PET to 100% in high-grade gliomas and accuracy of ^{1}H-MRS to 80% in low-grade tumors. Spearman's analysis demonstrated a trend between ^{18}F-FDG uptake and tumor grading ($\rho = 0.612$, p-value = 0.272). The results of ^{18}F-FDG-PET and ^{1}H-MRS were concordant in 75% (9/12) of cases.

Conclusion—The combination of ^{1}H-MRS data and ^{18}F-FDG-PET imaging can enhance detection of glioma progression. ^{1}H-MRS imaging was more accurate in low-grade gliomas and ^{18}F-FDG-PET provided better accuracy in high-grade gliomas.

INTRODUCTION

The Central Brain Tumor Registry of the United States estimates that 62,930 new cases of primary non–malignant and malignant brain and central nervous system tumors are expected to be diagnosed in the United States in 2010. Ninety three percent of cases are individuals over 20 years old at the time of diagnosis and gliomas account for 80% of malignant brain tumors1, 2.

Most gliomas are characterized by diffuse infiltration of white matter tracts 3. Stereotactic biopsy studies have shown tumor infiltration in regions that appear normal on conventional contrast enhanced computed tomography (CT) and magnetic resonance imaging (MRI) 4. Eradication of the tumors, particularly higher grade neoplasms, is not usually possible 5. Thus, post-therapy imaging to detect the presence of residual or recurrent tumor is essential to optimize patient management. Assessments of tumor response to therapy are typically performed by visual interpretation of serial MRI examinations. Although such examinations provide useful morphologic information, they are not able to reliably distinguish active

tumor from radiation necrosis. Anatomic distortion, scarring, altered vascular permeability and edema after therapy often impair interpretation of conventional CT and contrast enhanced MRI studies.

Metabolite and molecular imaging methods can help overcome this issue. Specific biologic information provided by ^{1}H MRS such as cell membrane turnover 6, cellular density 7 and proliferation 8 as well as, glucose metabolism quantified by ^{18}F-FDG PET imaging 9 may distinguish glioma progression from post-radiation changes.

Although numerous ^{1}H MRS 10-20 and ^{18}F-FDG PET 21-30 studies have been conducted in order to describe metabolite and metabolic patterns of brain tumors, (Table 1), only a few investigations focused on detecting tumor progression by evaluating both ^{1}H MRS and ^{18}F-FDG PET data in the same group of patients 31, 32. While these studies have provided valuable results, their methods could be further improved in several aspects. These studies did not attempt to co-register ^{18}F-FDG PET images with MRI which has been shown to significantly improve sensitivity and specificity of distinguishing recurrent brain tumors from radionecrosis 33. The differences between grades of malignancy were not evaluated. Alger et al. focused on single voxel analysis of ^{1}H MRS. They preferred to employ larger volumes rather than smaller, to maximize the probability of including the most active part of the tumor in the MR spectroscopy. Distinction between necrosis resulting from therapy and tumor regrowth was difficult in this study. Therefore, the statistical measures of the performance were not reported. In recent years, multispectral analysis of ^{1}H MRS data that allows mapping the metabolite concentrations have significantly improved clinical application of this technique 34.

The main aim of our study was to assess and compare the contribution of ^{1}H MRS and ^{18}F-FDG PET to non-invasively differential grades II and III glioma progression from necrosis. The specific focus of this study was to detect lesions by visual analysis of ^{1}H MRS data presented as 3D maps of metabolites and ^{18}F-FDG PET images co-registered with MRI.

MATERIALS AND METHODS

Inclusion and Exclusion Criteria

Subjects for this study were drawn from a total of 193 patients who were referred from our neurooncology group for a conventional clinical brain MRI during the period from 3/2007 to 3/2009. From this group 53 patients had a history of grade II or grade III glioma resection, stereotactic radiation and chemotherapy. Patients with no evidence of progression (N = 24) and cases demonstrating significant tumor growth were excluded (N = 3) from further consideration, since their clinical status was considered stable or definite progression from the clinical MRI scan and/or symptoms. The remaining patients (n= 26), had clinical symptoms and radiographic findings suspicious but not conclusive for glioma progression, and were referred for an ^{18}F-FDG PET scan. All patients in this group were adult male or female patients older than 20 years.

In western Pennsylvania, third party payer constraints on coverage for MRS limit the use of MRS for brain tumor indications. UPMC Health Plan has followed the recommendations of the Neurooncology Program faculty and provides coverage for patients with primary brain tumors undergoing MRS as part of clinical care. The seventeen patients who had UPMC health insurance were also evaluated by 3T ^{1}H MRS. In most cases the MRS and PET scans were ordered at approximately the same time, and therefore either ^{1}H MRS or ^{18}F-FDG PET could have been performed first and in all cases no patient was excluded on the basis of ^{1}H MRS and ^{18}F-FDG PET findings. Of the total of 17 ^{1}H MRS scans, five cases were excluded from data analysis because the time interval between the two studies was longer

than one month. Twelve cases (5 men, 7 women; median age at surgery 39; range, 25–70 years) were selected for the study.

A combination of clinical follow-up and multiple sequential MR studies were used for clinical outcome validation. This retrospective study was approved by our Institutional Review Board which did not require signed informed consent from the patients.

Magnetic Resonance Spectroscopy Imaging

MRI and MRS data were acquired on a Siemens (Erlangen, Germany) 3T Magnetom TIM Trio whole-body high-performance scanner. The patients were positioned in the standard radiofrequency (RF) 12-channel head coil. A fast 3D gradient echo sequence (MP-RAGE) was performed using a TE of 2.63ms, TR of 2110ms, inversion time of 1100ms, flip angle of 8 degrees, image matrix 256^2, 128 slices 1.5mm thick and a 240×192 field of view, resulting in a scan time of 3.8 min. Parallel acquisition techniques (PAT) factor of 2 was used to decrease the imaging time. These parameters resulted in images optimized for the best contrast among gray matter, white matter, and CSF and to provide high-resolution delineation of cortical and sub-cortical structures.

The ^{1}H MRS data were acquired using a hybrid chemical shift imaging (CSI) sequence with TE of 135ms, TR of 1700 ms, slice thickness of 10mm and three averages over a 160×160mm field of view, resulting in a scan time of 6.8 min. Outer volume suppression pulses were used to suppress subcutaneous lipid signals. The positioning of the CSI slice was dependent on the location of the lesion. An automatic 3D shimming was used to maximize spectral resolution and homogeneity over the volume of interest. Water suppression was performed using the vendor-supplied adjustment employing a special pulse train.

Integrals of resonance signals (areas under the peaks) were obtained after baseline correction and phase correction were applied to all the spectra. This allowed for visualization of the voxel-dependent intensities of metabolites within the defined region of interest. Metabolite images were generated on the scanner console using routines provided by the manufacturer. The CSI slice graphic was displayed as an overlay on the MP-RAGE sequence.

Positron Emission Tomography Method

The patients were instructed to fast for 4–6 hours before the injection of 353–532 MBq (9.5–14.4 mCi) of ^{18}F-FDG. The PET data were acquired on a Siemens/CTI ECAT HR+ scanner in 3D imaging mode (63 parallel planes); axial field-of-view: 15.2 cm; in-plane resolution: 4.1 mm full-width at half-maximum; slice width: 2.4 mm). The scanner gantry was equipped with a Neuro-insert (CTI PET Systems, Knoxville, TN) to reduce the contribution of scattered photon events35. PET data were reconstructed using filtered back-projection (Fourier rebinning and 2D back projection with Hann filter: kernel FWHM = 3 mm). Data were corrected for photon attenuation, scatter, and radioactive decay. A windowed transmission scan (10–15 min) was obtained for attenuation correction using rotating 68Ge/68Ga rods and a model-based correction was applied to account for a 3D scatter fraction36.

Interpretation of MRS and PET Studies

All ^{1}H MRS and ^{18}F-FDG PET images were interpreted by two examiners. One examiner was board certified in radiology and nuclear medicine and the other examiner was board certified in nuclear medicine. The images were reviewed using image analysis and fusion software (MIMvista Corp. Cleveland, OH). The interpreters were unaware of the patients' clinical history and prior imaging studies.

Quantitative analysis of ^{1}H MRS data was performed by placing a region of interest composed of 64 voxels over the tumor visually. Metabolite levels of each voxel (1.6 • 1.6 • 1.6 cm^3) were obtained by integration of the area under peaks. The voxel with the highest choline to creatine ratio (Cho/Cr) was selected and compared to the normal contralateral hemisphere. Three-dimensional maps of Cho/Cr were generated on a semiquantitative scale and co-registered with MR images for visual interpretation as illustrated in figure 1. The observers favored tumor progression versus necrosis with use of the following criteria: (a) Presence of spectra with interpretable signal intensities. (b) Cho/Cr signal ratio of the tumor substantially higher than that of the normal contralateral hemisphere. (c) A decrease in the NAA signal intensity. (d) Visible lactate signal in the spectrum.

PET images were co-registered with MRI to better localize the lesions (Figure 1). ^{18}F-FDG PET studies were considered either positive or negative semi-quantitatively by comparing metabolic activity of the lesions with the normal white and gray matters. Based on visual inspection, the examiners graded the highest activity level of the tumor using the metabolic grading; 0, no discernible uptake; 1, uptake less or equal to normal white matter; 2, uptake greater than normal white matter and less than gray matter; 3, uptake equal to or greater than gray matter[37, 38]. The examiners favored tumor progression for lesions with metabolic activity of grade 2 and 3.

Both examiners evaluated all ^{1}H MRS and ^{18}F-FDG PET studies independently in the same session. Selected voxels for quantitative analysis were visually examined to represent the same lesion. The examiners agreed on all cases except one MRS study (case 9), which was subsequently discussed and reached consensus.

Composite Reference

Histological verification, which would have been the most accurate reference standard, was not feasible in all cases. Therefore, a combination of follow-up clinical evaluations and multiple sequential MR studies were used as the reference standard to determine the accuracy of ^{1}H MRS and ^{18}F-FDG PET in the diagnosis of progression.

Statistical Analysis

Data were divided into two groups of high-grade and low-grade gliomas. Sensitivity, specificity, and accuracy with 95% confidence interval (CI) were calculated [39-42] for each group as well as the combined data using the composite reference standard. Concordance between ^{1}H MRS and ^{18}F-FDG PET grading was assessed by the McNemar's Exact test. For correlation between ^{18}F-FDG uptake and tumor grading, the Spearman nonparametric correlation coefficient was calculated. The ^{18}F-FDG uptake and Cho/Cr ratio of low-grade and high-grade tumors were compared using the Mann–Whitney nonparametric analysis. A 2-sided p-value of less than 0.05 was considered significant.

RESULTS

Twelve cases were selected for the study. Six patients had glioma grade II and six patients had glioma grade III on the basis of initial histological diagnosis (Table 2). All suspicious cases demonstrated post-contrast enhancement on MRI studies expect one (case 6), who showed progressive increase in fluid-attenuated inversion recovery (FLAIR) signal at the margins of the resection cavity on two consecutive MRI studies. Metabolites and metabolic evaluation of the lesions were performed for all patients within one month. MRS preceded PET in five cases. In another five cases PET preceded MRS and in two cases both studies were performed on the same day (mean and median time intervals from radiation therapy to scan were 18 months and 13 months respectively, range, 42 days–9 years).

Two patients (cases 1 and 5) had subsequent brain biopsies which revealed glioma progression. The remaining nine patients had a minimum of 12 months follow-up. Sequential imaging studies and clinical assessments demonstrated glioma progression in three of these patients. Seven patients did not show any clinical or radiographic evidence of progression during the observation period.

The sensitivity of ^{1}H MRS for diagnosis of glioma progression was 80% (95% CI, 30% to 99%). ^{18}F-FDG PET demonstrated no false negative findings. Therefore, sensitivity of ^{18}F-FDG PET was 100% (95% CI, 46% to 100%). The specificity of ^{1}H MRS and ^{18}F-FDG PET was 71% (95% CI, 30% to 95%) for both studies. The accuracy of ^{1}H MRS and ^{18}F-FDG PET studies was 75% (95% CI, 43% to 93%) and 83% (95% CI, 51% to 97%), respectively. Classifying the tumors into high and low grade gliomas improved accuracy of ^{1}H MRS studies to 80% (95% CI, 30% to 95%) in low-grade gliomas and accuracy of ^{18}F-FDG PET to 100% (95% CI, 56% to 100%) in high-grade gliomas (Table 3).

Concordance analysis using McNemar's Exact test did not show statistically significant difference between the two methods (p-value = 0.625). The results of ^{1}H MRS and ^{18}F-FDG PET were concordant in 75% (9/12) of cases (Table 4).

Prior studies reported a positive correlation between metabolic rate of glucose and histological grade of cerebral gliomas before initiation of treatment 42, 43. We obtained similar results in post-therapy patients with recurrent gliomas. There was a trend toward positive correlation between tumor grading and ^{18}F-FDG uptake; however it did not reach statistical significance level (Spearman $\rho = 0.612$, $p = 0.272$). No correlation was identified between tumor grading and Cho/Cr.

DISCUSSION

To our knowledge this is the first clinical study to compare ^{1}H MRS data presented in semiquantitative 3D maps of Cho/Cr and ^{18}F-FDG PET imaging to detect glioma progression from necrosis. Radiation necrosis following radiation therapy for treatment of gliomas is not uncommon and has been well described in autopsy and imaging studies 44, 45. Similarities with conventional imaging characteristics of glioma progression, including contrast enhancement, mass effect, and vasogenic edema have confounded differential diagnostic evaluation. Advanced imaging techniques including proton magnetic resonance spectroscopy and positron emission tomography have increased diagnostic accuracy. As illustrated in the figure 1, ^{1}H MRS and ^{18}F-FDG PET offer different information about the tumors. ^{1}H MRS primarily provides a measure of the tissue concentrations of various metabolites, including choline, creatine, N-acetylaspartate and lactate. Choline is the main metabolite that has been assessed in gliomas. Increased choline levels are associated with higher cell membrane turnover and higher cell density 7, arising from the proliferation of tumor cells 8. Creatine plays a role in maintaining energy-dependent systems in cells. It is the most stable cerebral metabolite 46 and is used as internal reference value. An increase in Cho/Cr ratio is suggestive of neoplastic process. In order to facilitate simultaneous visual analysis of multiple-voxel spectra, Cho/Cr maps of the regions of interest were generated as shown in figure 1. The examiners favored tumor progression for the lesions with increased Cho/Cr compared with the contralateral hemisphere. This approach, in contrast to the prior studies that focused on spectrum analysis of a single voxel, can expedite the diagnostic process and provide a more practical approach in the clinical setting. The examiners also evaluated the NAA and lactate resonances. NAA is a marker of neuronal viability and density. It is localized in mature neurons and is not found in glial cells 47, 48. Lactate peak represents anaerobic glycolysis in tumors 34 which has been shown to increase in neoplastic

cells 49. A decrease in NAA and a visible lactate peak were also considered as evidence of tumor progression.

^{18}F-FDG PET can measure the rate at which the glucose is consumed. Most cancer cells including gliomas produce energy by a high rate of glycolysis 49, quantifiable by ^{18}F-FDG PET imaging. We co-registered all ^{18}F-FDG PET studies with MRI images which have been shown to significantly improve diagnostic accuracy of distinguishing recurrent brain tumors from radionecrosis 33.

Our results demonstrate that ^{1}H MRS imaging is more accurate in detecting low-grade glioma progression and high-grade gliomas are better detected by ^{18}F-FDG PET. Classifying the tumors by grade improved the accuracy of ^{1}H MRS from 75% to 80% in low-grade gliomas. In addition, accuracy of ^{18}F-FDG PET increased from 83% to 100% in high-grade gliomas (Table 3). While the sensitivity of ^{18}F-FDG PET in detecting glioma progression was very high (100%), its specificity in differentiating post-therapy inflammation from true tumor progression was low (71%), leading to high false positive rate (29%) in post radiation therapy patients.

In our study, ^{1}H MRS and ^{18}F-FDG PET were concordant in 75% (9/12) of patients. In the three discordant cases, ^{18}F-FDG PET imaging confirmed tumor progression at the margins of the resection cavity in a patient with a history of high grade glioma (case 3). PET also correctly showed an absence of abnormal metabolic activity in the region of prior tumor resection in a patient with a history of high-grade glioma. This patient did not show any evidence of progression during more than a two-year follow-up (case 2). In the third discordant case, ^{1}H MRS correctly diagnosed tumor progression in a previously treated low-grade glioma (case 8). Failure in detecting viable tumors on ^{18}F-FDG PET imaging could be due to several factors, including high rate of glucose metabolism by the normal brain tissue, small size of the lesions, and modest increase in glucose metabolism in low-grade gliomas (relative to the background metabolic activity) 28, 43.

This study has several limitations. Histopathologic confirmation of tumor progression was not performed for all cases. Because of the inherent risks and invasiveness of a stereotactic biopsy, it was not always reasonable to obtain histological proof. Only two cases had subsequent tissue biopsy (cases 1 and 5). Sequential morphologic imaging and prolonged clinical follow-up had to be used as surrogate markers for tissue identification in the remainder of patients. Second, we were not able to confirm possibility of high-grade transformation. All data were analyzed based on the patients' last histopathology report. Third limitation is the relatively small number of patients in this study. Finally, the current study did not attempt a comparison with other biomarkers, such as 3′-deoxy-3′-^{18}F-fluorothymidine (^{18}F-FLT) and 3,4-dihydroxy-6-^{18}F-fluoro-L-phenylalanine (^{18}F-FDOPA).

In conclusion, the combination of ^{1}H MRS data and ^{18}F-FDG PET imaging improves the accuracy of distinguishing glioma progression from radionecrosis. ^{18}F-FDG PET was more accurate in identifying tumor progression in high-grade gliomas and Cho/Cr ^{1}H MRS provided better accuracy in low-grade gliomas. Proton MR spectroscopy and ^{18}F-FDG PET appear to be useful complementary tools to conventional MR imaging in detecting brain tumor progression.

Acknowledgments

This work was support by the US National Institutes of Health research grants R01 CA106840 and U01 CA140230.

The authors thank the technology staff of the University of Pittsburgh Medical Center PET-Cyclotron facility and MR Research Center for expert adherence to PET and MRI scan acquisition protocols.

REFERENCES

1. CBTRUS. Central Brain Tumor Registry of the United States Statistical Report: Primary Brain and Central Nervous System Tumors Diagnosed in the United States in 2004-2006. 2010
2. kKleihues, P.; Cavenee, WK.; International Agency for Research on Cancer. Pathology and genetics of tumours of the nervous system. IARC Press; Lyon: 2000.
3. Kelly PJ, Daumas-Duport C, Scheithauer BW, Kall BA, Kispert DB. Stereotactic histologic correlations of computed tomography- and magnetic resonance imaging-defined abnormalities in patients with glial neoplasms. Mayo Clin Proc. Jun; 1987 62(6):450–459. [PubMed: 3553757]
4. Earnest, Ft; Kelly, PJ.; Scheithauer, BW., et al. Cerebral astrocytomas: histopathologic correlation of MR and CT contrast enhancement with stereotactic biopsy. Radiology. Mar; 1988 166(3):823–827. [PubMed: 2829270]
5. Buckner JC, Brown PD, O'Neill BP, Meyer FB, Wetmore CJ, Uhm JH. Central nervous system tumors. Mayo Clin Proc. Oct; 2007 82(10):1271–1286. [PubMed: 17908533]
6. Danielsen, ER.; Ross, B. Magnetic Resonance Spectroscopy Diagnosis of Neurological Diseases. CRC Press; 1999.
7. Michaelis T, Merboldt KD, Bruhn H, Hanicke W, Frahm J. Absolute concentrations of metabolites in the adult human brain in vivo: quantification of localized proton MR spectra. Radiology. Apr; 1993 187(1):219–227. [PubMed: 8451417]
8. Herminghaus S, Pilatus U, Moller-Hartmann W, et al. Increased choline levels coincide with enhanced proliferative activity of human neuroepithelial brain tumors. NMR Biomed. Oct; 2002 15(6):385–392. [PubMed: 12357552]
9. Tewson TJ, Welch MJ, Raichle ME. [18F]-labeled 3-deoxy-3-fluoro-D-glucose: synthesis and preliminary biodistribution data. J Nucl Med. Dec; 1978 19(12):1339–1345. [PubMed: 104019]
10. Senft C, Hattingen E, Pilatus U, et al. Diagnostic value of proton magnetic resonance spectroscopy in the noninvasive grading of solid gliomas: comparison of maximum and mean choline values. Neurosurgery. Nov; 2009 65(5):908–913. discussion 913. [PubMed: 19834403]
11. Fayed N, Davila J, Medrano J, Olmos S. Malignancy assessment of brain tumours with magnetic resonance spectroscopy and dynamic susceptibility contrast MRI. Eur J Radiol. Sep; 2008 67(3): 427–433. [PubMed: 18442889]
12. Zonari P, Baraldi P, Crisi G. Multimodal MRI in the characterization of glial neoplasms: the combined role of single-voxel MR spectroscopy, diffusion imaging and echo-planar perfusion imaging. Neuroradiology. Oct; 2007 49(10):795–803. [PubMed: 17619871]
13. Zeng QS, Li CF, Zhang K, Liu H, Kang XS, Zhen JH. Multivoxel 3D proton MR spectroscopy in the distinction of recurrent glioma from radiation injury. J Neurooncol. Aug; 2007 84(1):63–69. [PubMed: 17619225]
14. Law M, Yang S, Wang H, et al. Glioma grading: sensitivity, specificity, and predictive values of perfusion MR imaging and proton MR spectroscopic imaging compared with conventional MR imaging. AJNR Am J Neuroradiol. Nov-Dec; 2003 24(10):1989–1998. [PubMed: 14625221]
15. Reijneveld JC, van der Grond J, Ramos LM, Bromberg JE, Taphoorn MJ. Proton MRS imaging in the follow-up of patients with suspected low-grade gliomas. Neuroradiology. Dec; 2005 47(12): 887–891. [PubMed: 16133483]
16. Lichy MP, Plathow C, Schulz-Ertner D, Kauczor HU, Schlemmer HP. Follow-up gliomas after radiotherapy: 1H MR spectroscopic imaging for increasing diagnostic accuracy. Neuroradiology. Nov; 2005 47(11):826–834. [PubMed: 16142479]
17. Floeth FW, Pauleit D, Wittsack HJ, et al. Multimodal metabolic imaging of cerebral gliomas: positron emission tomography with [18F]fluoroethyl-L-tyrosine and magnetic resonance spectroscopy. J Neurosurg. Feb; 2005 102(2):318–327. [PubMed: 15739561]
18. Fayed N, Modrego PJ. The contribution of magnetic resonance spectroscopy and echoplanar perfusion-weighted MRI in the initial assessment of brain tumours. J Neurooncol. May; 2005 72(3):261–265. [PubMed: 15937650]
19. Plotkin M, Eisenacher J, Bruhn H, et al. 123I-IMT SPECT and 1H MR-spectroscopy at 3.0 T in the differential diagnosis of recurrent or residual gliomas: a comparative study. J Neurooncol. Oct; 2004 70(1):49–58. [PubMed: 15527107]

20. McKnight TR, von dem Bussche MH, Vigneron DB, et al. Histopathological validation of a three-dimensional magnetic resonance spectroscopy index as a predictor of tumor presence. J Neurosurg. Oct; 2002 97(4):794–802. [PubMed: 12405365]
21. Patronas NJ, Di Chiro G, Brooks RA, et al. Work in progress: [18F] fluorodeoxyglucose and positron emission tomography in the evaluation of radiation necrosis of the brain. Radiology. Sep; 1982 144(4):885–889. [PubMed: 6981123]
22. Doyle WK, Budinger TF, Valk PE, Levin VA, Gutin PH. Differentiation of cerebral radiation necrosis from tumor recurrence by [18F]FDG and 82Rb positron emission tomography. J Comput Assist Tomogr. Jul-Aug; 1987 11(4):563–570. [PubMed: 3496366]
23. Di Chiro G, Oldfield E, Wright DC, et al. Cerebral necrosis after radiotherapy and/or intraarterial chemotherapy for brain tumors: PET and neuropathologic studies. AJR Am J Roentgenol. Jan; 1988 150(1):189–197. [PubMed: 3257119]
24. Valk PE, Budinger TF, Levin VA, Silver P, Gutin PH, Doyle WK. PET of malignant cerebral tumors after interstitial brachytherapy. Demonstration of metabolic activity and correlation with clinical outcome. J Neurosurg. Dec; 1988 69(6):830–838. [PubMed: 2848111]
25. Kim EE, Chung SK, Haynie TP, et al. Differentiation of residual or recurrent tumors from post-treatment changes with F-18 FDG PET. Radiographics. Mar; 1992 12(2):269–279. [PubMed: 1561416]
26. Janus TJ, Kim EE, Tilbury R, Bruner JM, Yung WK. Use of [18F]fluorodeoxyglucose positron emission tomography in patients with primary malignant brain tumors. Ann Neurol. May; 1993 33(5):540–548. [PubMed: 8498831]
27. Kahn D, Follett KA, Bushnell DL, et al. Diagnosis of recurrent brain tumor: value of 201Tl SPECT vs 18F-fluorodeoxyglucose PET. AJR Am J Roentgenol. Dec; 1994 163(6):1459–1465. [PubMed: 7992747]
28. Ricci PE, Karis JP, Heiserman JE, Fram EK, Bice AN, Drayer BP. Differentiating recurrent tumor from radiation necrosis: time for re-evaluation of positron emission tomography? AJNR Am J Neuroradiol. Mar; 1998 19(3):407–413. [PubMed: 9541290]
29. Van Laere K, Ceyssens S, Van Calenbergh F, et al. Direct comparison of 18F-FDG and 11C-methionine PET in suspected recurrence of glioma: sensitivity, inter-observer variability and prognostic value. Eur J Nucl Med Mol Imaging. Jan; 2005 32(1):39–51. [PubMed: 15309329]
30. Wang SX, Boethius J, Ericson K. FDG-PET on irradiated brain tumor: ten years' summary. Acta Radiol. Feb; 2006 47(1):85–90. [PubMed: 16498938]
31. Alger JR, Frank JA, Bizzi A, et al. Metabolism of human gliomas: assessment with H-1 MR spectroscopy and F-18 fluorodeoxyglucose PET. Radiology. Dec; 1990 177(3):633–641. [PubMed: 2243962]
32. Prat R, Galeano I, Lucas A, et al. Relative value of magnetic resonance spectroscopy, magnetic resonance perfusion, and 2-((18)F) fluoro-2-deoxy-D-glucose positron emission tomography for detection of recurrence or grade increase in gliomas. J Clin Neurosci. Dec 1.2009
33. Chao ST, Suh JH, Raja S, Lee SY, Barnett G. The sensitivity and specificity of FDG PET in distinguishing recurrent brain tumor from radionecrosis in patients treated with stereotactic radiosurgery. Int J Cancer. Jun 20; 2001 96(3):191–197. [PubMed: 11410888]
34. Castillo M, Kwock L, Mukherji SK. Clinical applications of proton MR spectroscopy. AJNR Am J Neuroradiol. Jan; 1996 17(1):1–15. [PubMed: 8770242]
35. Weinhard, K. The theory and practice of 3D PET. Kluwer Academic; Dordrecht ; Boston: 1998. Applications of 3D PET. In: Bendriem B, Townsend DW, eds; p. 133-167.
36. Watson CC. New, faster, image-based scatter correction for 3D PET. Nuclear Science, IEEE Transactions on. 2000; 47(4):1587–1594.
37. Padma MV, Said S, Jacobs M, et al. Prediction of pathology and survival by FDG PET in gliomas. J Neurooncol. Sep; 2003 64(3):227–237. [PubMed: 14558598]
38. Meyer PT, Schreckenberger M, Spetzger U, et al. Comparison of visual and ROI-based brain tumour grading using 18F-FDG PET: ROC analyses. Eur J Nucl Med. Feb; 2001 28(2):165–174. [PubMed: 11303886]

39. Julious SA. Two-sided confidence intervals for the single proportion: comparison of seven methods by Robert G. Newcombe, Statistics in Medicine 1998; 17:857-872. Stat Med. Nov 15; 2005 24(21):3383–3384. [PubMed: 16206245]
40. Newcombe RG. Two-sided confidence intervals for the single proportion: comparison of seven methods. Stat Med. Apr 30; 1998 17(8):857–872. [PubMed: 9595616]
41. Wilson EB. Probable Inference, the Law of Succession, and Statistical Inference. Journal of the American Statistical Association,. Jun.; 1927 22(158):209–212. 1927.
42. Vollset SE. Confidence intervals for a binomial proportion. Stat Med. May 15; 1993 12(9):809–824. [PubMed: 8327801]
43. Olivero WC, Dulebohn SC, Lister JR. The use of PET in evaluating patients with primary brain tumours: is it useful? J Neurol Neurosurg Psychiatry. Feb; 1995 58(2):250–252. [PubMed: 7876865]
44. Burger PC, Mahley MS Jr. Dudka L, Vogel FS. The morphologic effects of radiation administered therapeutically for intracranial gliomas: a postmortem study of 25 cases. Cancer. Oct; 1979 44(4): 1256–1272. [PubMed: 387205]
45. Marks JE, Baglan RJ, Prassad SC, Blank WF. Cerebral radionecrosis: incidence and risk in relation to dose, time, fractionation and volume. Int J Radiat Oncol Biol Phys. Feb; 1981 7(2):243–252. [PubMed: 6260715]
46. Kreis R, Ernst T, Ross BD. Development of the human brain: in vivo quantification of metabolite and water content with proton magnetic resonance spectroscopy. Magn Reson Med. Oct; 1993 30(4):424–437. [PubMed: 8255190]
47. Miller BL. A review of chemical issues in 1H NMR spectroscopy: N-acetyl-L-aspartate, creatine and choline. NMR Biomed. Apr; 1991 4(2):47–52. [PubMed: 1650241]
48. Castillo M, Kwock L, Scatliff J, Mukherji SK. Proton MR spectroscopy in neoplastic and non-neoplastic brain disorders. Magn Reson Imaging Clin N Am. Feb; 1998 6(1):1–20. [PubMed: 9449737]
49. Warburg O. On the origin of cancer cells. Science. Feb 24; 1956 123(3191):309–314. [PubMed: 13298683]

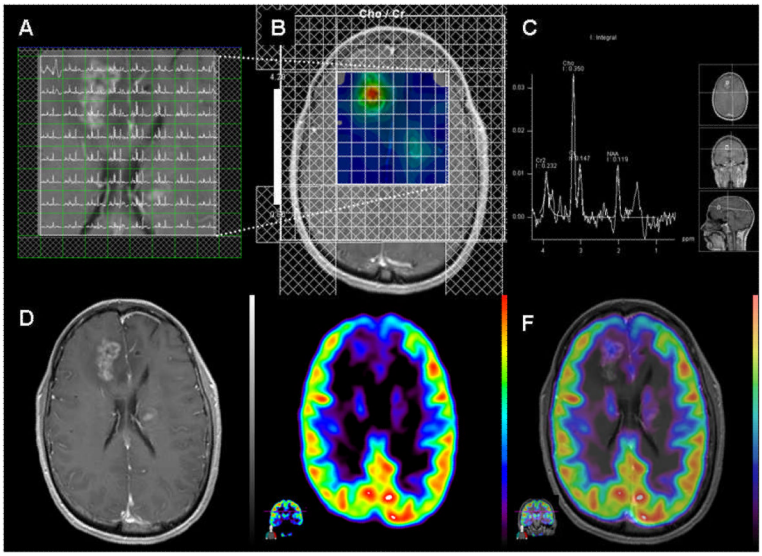

Figure 1.

Anaplastic Astrocytoma, WHO grade III (case 5). A. Multiple-voxel spectra co-registered with post-contrast T1-weighted MRI B. Map of Cho/Cr demonstrates a focus of signal intensity in the right frontal lobe. MRSI signal intensity is presented on a rainbow color scale where blue-green is normal background and bright red corresponds to greatly elevated signal intensity. C. Spectral analysis of the voxel demonstrating maximal Cho/Cr ratio. D. T1-weighted MRI (post-contrast) demonstrating enhancing lesion in the right frontal lobe. E. ^{18}F-FDG PET scan shows a focus of increased tracer activity greater than white matter in the right frontal lobe. F. ^{18}F-FDG PET image co-registered with post-contrast T1-weighted MRI.

Table 1

Accuracy of PET and MRS in differentiation of radiation injury from tumor progression

	Author	Year	Histology	N	Sensitivity	Specificity	Accuracy	Parameters
MRS	Law	2003	High-grade	43	76%	48%	69%	Cho/Cr
	Law		High grade	160	74%	63%	71%	Cho/NAA
	Plotkin	2004	Glioma	25	89%	83%	88%	Cho/Cr
	Lichy	2005	Glioma	34	81%	71%		Cho/Cr and Cho/NAA
	Zeng	2007	High-grade	28	94%	100%	96%	Cho/Cr and Cho/NAA
	Prat	2010	Glioma	9	100%	100%	100%	Cho and NAA
PET	Patronas	1982	Low-grade	5	100%	100%	100%	
	Doyle	1987	High-grade	9	100%	100%	100%	
	Di Chiro	1988	Glioma	95	100%	100%	100%	
	Valk	1988	Glioma	38	81%	88%	86%	
	Kim	1992	Glioma	33	80%	94%	88%	
	Janus	1993	Glioma	20	83%	63%	75%	
	Kahn	1994	Glioma	17	81%	40%		
	Ricci	1998	Glioma	31	86%	22%	71%	
	Van Laere	2004	Glioma	30	80%	95%	50%	
	Wang	2006	Glioma	129	80%	96%	87%	
	Prat	2010	Glioma	9	50%	75%	63%	

Table 2

Demographic data and history

No.	Age (years) at Surgery	Sex	Histology	WHO Grade	Interval Since Radiation (months)	PET-MRS Interval (days) *	Necrosis versus Progression
1	49	M	Anaplastic Astrocytoma	3	10	3	Necrosis
2	29	F	Anaplastic Oligodendroglioma	3	7	0	Necrosis
3	45	M	Anaplastic Astrocytoma	3	111	22	Progression
4	29	M	Anaplastic Astrocytoma	3	1	0	Progression
5	30	F	Oligodendroglioma	2	8	19	Progression
6	54	F	Astrocytoma	2	19	−14	Progression
7	60	F	Oligodendroglioma	2	1	−15	Progression
8	70	F	Oligodendroglioma	2	2	5	Necrosis
9	30	M	Oligodendroglioma	2	17	−1	Necrosis
10	25	F	Astrocytoma	2	14	−1	Necrosis
11	60	F	Anaplastic Astrocytoma	3	17	−7	Necrosis
12	33	M	Anaplastic Astrocytoma	3	13	11	Necrosis

* Positive numbers demonstrate MRS preceded PET and negative numbers show MRS was performed after PET.

Table 3

Statistical measures of the performance of ^{18}F-FDG PET and ^{1}H MRS

Visual Analysis	Parameter (%)	All Cases	Low–Grade	High–Grade
^{18}F-FDG PET	**Sensitivity**	80 (30–99)	100 (20–100)	67 (13–98)
	Specificity	71 (30–95)	67 (13–98)	75 (22–99)
	PPV	83 (36–99)	100 (20–100)	75 (22–99)
	NPV	67 (24–94)	67 (13–98)	67 (13–98)
	Accuracy	75 (43–93)	80 (30–99)	71 (30–95)
^{1}H MRS	**Sensitivity**	100 (46–100)	100 (20–100)	100 (31–100)
	Specificity	71 (30–95)	33 (2–87)	100 (40–100)
	PPV	100 (46–100)	100 (5–100)	100 (40–100)
	NPV	71 (30–95)	50 (9–91)	100 (31–100)
	Accuracy	83 (51–97)	60 (17–93)	100 (56–100)

* Numbers in parentheses are 95% confidence intervals.

Table 4

Concordance between PET and MRSI

		MRSI		
Concordance		**Progression**	**No progression**	
PET	Progression	5	2	Concordance = 75% (9/12) p-value = 0.625
	No progression	1	4	

The concordance results are based on the experts' analyses of MRSI and PET studies.